Bifurcation of a Coastal Current at an Escarpment

GEORGE F. CARNEVALE

Scripps Institution of Oceanography, University of California, San Diego, La Jolla, California

STEFAN G. LLEWELLYN SMITH

Department of Applied Mathematics and Theoretical Physics, University of Cambridge, Cambridge, United Kingdom

FULVIO CRISCIANI AND ROBERTO PURINI

Istituto Talassografico-CNR, Trieste, Italy

ROBERTA SERRAVALL

Department of Mechanics and Aeronautics, University of Rome, La Sapienza, Rome, Italy

(Manuscript received 28 July 1997, in final form 16 June 1998)

ABSTRACT

The evolution of a coastal current as it encounters an escarpment depends strongly on whether the geometry of the coast and escarpment is right or left ''handed,'' independent of the direction of the coastal current. Handedness is defined such that right-handed means that when looking across the escarpment from the deep to the shallow side, the coast is found on the right. The essential aspects of the difference in behavior of the current in the two geometries are captured by a simple quasigeostrophic model of coastal flow over a step. An exact analytic solution to the nonlinear stationary problem is obtained. This solution shows that, when a coastal current crosses an escarpment in the left-handed geometry, the speed of the current will increase independent of whether the flow is from shallow to deep or from deep to shallow. For the right-handed geometry, the speed of the current decreases, also independent of the direction of the coastal flow. In the left (right)-handed geometry, there is associated to the coastal flow an inshore (offshore) current along the escarpment. These results are explained in terms of linear wave theory and vortex dynamics. Numerical simulations are used to examine the evolution of the flow from the initial encounter to the establishment of a stationary flow. The relevance of this research is discussed in light of recent results from laboratory experiments and oceanic observations.

1. Introduction

The presence of an escarpment, or step, may force a coastal current to bifurcate with one branch following the topographic contours of the step. As examples of this we can mention the Bering slope current (Kinder et al. 1986), the flow across the Adriatic Sea at the Jabuka Pit (Poulain, manuscript submitted to *J. Mar. Syst.*), flow along the Iceland–Faeroe Ridge (Hansen and Meincke 1979), and the Kuroshio as it follows the continental slope northeast of Taiwan (Hsueh et al. 1992; Stern and Austin 1995). In the ocean, many competing effects may tend to obscure this phenomenon. Coastline irregularity, complicated bottom topography, fluctuations in the wind, baroclinic instabilities, and other effects combine to make coastal current flow systems very complicated. Recent laboratory investigations have modeled the bifurcation with homogeneous flow over a simple step (Spitz and Nof 1991; Stern and Austin 1995). In these experiments, a wall jet is initiated from rest and then propagates along the wall of the tank before encountering a topographic step extending away from the wall. Even these highly simplified model flows present some interesting surprises. For example, instead of the expected simple bifurcation of the wall current at the step, Stern and Austin (1995) found that the current was partially reflected at the step back toward the source, with part continuing to follow the wall but with no flow along the slope. Spitz and Nof (1991) gave examples of simple coastal current bifurcations but in some cases observed strong eddy activity in the slope current. In what follows, we will present results of analytical and numerical investigations based on the qua-

Corresponding author address: Dr. George F. Carnevale, Scripps Institution of Oceanography, University of California, La Jolla, CA 92093-0225.
E-mail: gcarnevale@ucsd.edu

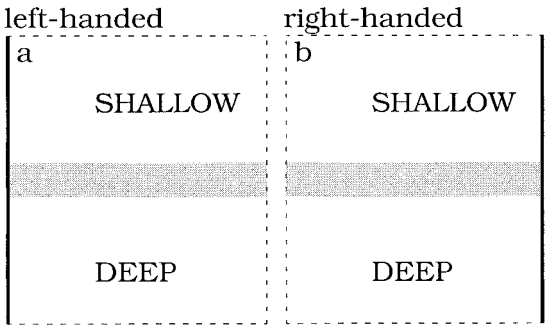

FIG. 1. Schematic of the flow over a step problem in the (a) left-handed and (b) right-handed geometries. The coastline is indicated by the solid lines. The open or inlet boundaries are indicated by dashed lines. The transition from deep to shallow fluid is indicated by the gray region where we assume a smooth slope.

sigeostrophic model that, we hope, will elucidate various aspects of this interesting problem.

The essential features of this problem are the presence of the coast, the step, and the background rotation. We will assume a finite background rotation rate of the system in a counterclockwise sense (Northern Hemisphere). There are two basic configurations of interest. The geometry of these is shown in plan form in Fig. 1. The coastlines are indicated by the thick solid lines, and the dashed lines indicate permeable or open boundaries. The topography changes from deep to shallow along the coast, and the topographic slope is indicated by the area shaded gray. We call these geometries left-handed or right-handed depending on the orientation of the topography with the coast line. If we look in the direction of the gradient of the topography, that is from deep to shallow, and the coast is on the left (right), then we refer to the geometry as left-handed (right-handed) (in the Northern Hemisphere). Another way to think of this is to consider the triad of vectors formed by the normal to the coastline (pointing out from the ocean), the horizontal gradient of topography, and the ambient rotation vector in that order. We call the geometry right-handed if this triad is right-handed. We then imagine a current flowing along the coast, coming initially from either the top or the bottom of the diagrams, with its course intercepted by the topographic step. The presence of the step may produce a bifurcation or even fully divert the current. The dynamical problem also shows the possibility of the generation of eddies when the current first encounters the slope. Due to the rotation, the flow in the left-handed geometry (Fig. 1a) will be fundamentally different from that in the right-handed geometry (Fig. 1b).

One way to appreciate the difference between the dynamics of flows in the right- and left-handed geometries is to consider the propagation of topographic Rossby waves in the system. We will consider the step to be made of a smooth slope of finite extent from the deep to shallow region. On this slope topographic Rossby waves will exist that have a direct analogy to Rossby waves on a β plane. The dispersion relation of Rossby waves on the β plane in a flow under a rigid lid is

$$\omega_{\mathbf{k}} = -\frac{\beta k_x}{k_x^2 + k_y^2}, \tag{1}$$

where the positive x direction corresponds to due east. Therefore, the group velocity is given by

$$\mathbf{c}_g = \frac{\beta}{(k_y^2 + k_x^2)^2}(k_x^2 - k_y^2,\ 2k_x k_y). \tag{2}$$

Thus, waves that are relatively long in the x direction (i.e., $|k_x/k_y| \ll 1$) will have a westward component of propagation, while waves that are relatively short in the x direction (i.e., $|k_x/k_y| \gg 1$) will have an eastward component of propagation (cf. Pedlosky 1965). In quasigeostrophic theory, the β effect is equivalent to the effect of a bottom slope of magnitude $f_0 m/H_0$, where f_0 is the Coriolis parameter, m the slope of the bottom in the y direction, and H_0 the mean depth of the fluid. Confining the extent of the slope in the y direction will change the dispersion relation somewhat (in particular the k_y values become discrete), but, nevertheless, the similarity with the dispersion relation (1) is sufficient to draw the same conclusion about propagation directions. Thus considering Fig. 1, in both the left- and right-handed cases as drawn, the topographic waves long in x will propagate toward the left, that is, toward the coast in the left-handed geometry and away from the coast in the right-handed geometry. Thus a disturbance caused by the interaction of a coastal flow over the topography should be expected to propagate very differently in the two geometries. Although this is only a part of the picture since the flows are nonlinear and flow structures other than waves will be found to play an important role, this view of the wave dynamics provides an important insight into the difference in the behavior of the flow in the two geometries.

The importance of the difference in the direction of propagation of the long topographic waves for the coastal escarpment problem has been pointed out in several previous articles, particularly in regard to the shallow-water version of the problem (cf. Rhines 1969; Johnson 1985; Gill et al. 1986; Willmott and Grimshaw 1991; Johnson and Davey 1990; Allen 1988, 1996; and Allen and Hsieh 1997). Many of the previous analytical studies focused on linear wave propagation in shallow-water theory. Although the propagation of topographic waves is an important part of the evolution of the flow, nonlinear effects can change the nature of the evolution and the long-term state significantly compared to the linear predictions. By using the quasigeostrophic model of this problem, we are able to present here a fully nonlinear steady-state solution, which has not appeared previously. This solution is very different from the corresponding solution obtained in linear shallow-water or quasigeostrophic theory as we will discuss below. In

addition, we will see how the transient evolution of the flow involves nonlinear coherent flow structures.

We begin, in the next section, by defining the step problem in the context of the quasigeostrophic model and providing some analytic solutions for the steady-state case. Then in section 3 we will compare these predictions to the results from numerical simulations. The simulations are performed with a finite-difference model that follows the evolution of a coastal current forced by inflow boundary conditions, from an initial state of no motion. Finally, in the discussion section, we will attempt to provide some physical insight into the differences for flow in the left-handed and right-handed geometries and also point out the connection to certain oceanographic observations.

2. An analytic steady-state solution

The simplest model of rotating flow that captures the essential ingredients of the coastal step problem is the barotropic quasigeostrophic model. The governing equation, which expresses the conservation of potential vorticity, may be written as

$$\frac{D}{Dt}(\omega + h) = 0, \tag{3}$$

or more explicitly as

$$\frac{\partial \omega}{\partial t} + J(\psi, \omega + h) = 0, \tag{4}$$

where ψ is the streamfunction, $\omega = \nabla^2\psi$ is the relative vorticity, and J is the Jacobian. The topographic term h is given by

$$h = -f\frac{\Delta H}{H_0}, \tag{5}$$

where H is the height of fluid column above the topography with the mean given by H_0. Thus,

$$H = H_0 + \Delta H = H_0\left(1 - \frac{h}{f}\right). \tag{6}$$

The sign convention for h is such that it is positive positive over hills and negative over valleys.

The appropriate form of the equation for steady flow is then

$$J(\psi, \nabla^2\psi + h) = 0. \tag{7}$$

The solution to this equation is

$$\nabla^2\psi + h = F(\psi) \tag{8}$$

for some function F, which simply means that the contours of potential vorticity, $\nabla^2\psi + h$, coincide with the contours of the streamfunction. The function F is, to some degree, determined by the boundary conditions, as will be discussed below.

The streamfunction may be decomposed into an unperturbed coastal current $\Psi(x)$ and a topographic response $\varphi(x, y)$, where we are using the traditional coordinate system with x running from left to right and y from bottom to top in the figures. We will begin by finding an analytic solution for the case where the coastal current is defined by a boundary condition at $y = -\infty$, where we will assume $\varphi = 0$. Alternate formulations with the boundary conditions at $y = +\infty$ will be discussed later. Only the gradient of the topography is important for (3) and not the absolute depth, and it will be convenient to take $h(x, -\infty) = 0$. Although it is not the only possibility, consider first the case in which F is defined to be the same function everywhere. Noting that there is no explicit dependence on position in (8), we consider it in the limit of $y \to -\infty$. There we have

$$\psi \equiv \Psi + \varphi \to \Psi \tag{9}$$

$$\nabla^2\psi + h \to \nabla^2\Psi. \tag{10}$$

Thus

$$\Psi_{xx}(x) = F(\Psi(x)). \tag{11}$$

The form of the unperturbed coastal current $\Psi(x)$ then determines the function F. Also, we see at this point that, if we had set $h(x, -\infty)$ to a constant value other than zero, this would have just altered the definition of F by a constant value.

The profile of coastal current that renders our problem most amenable to analysis is exponential. Accordingly, we take

$$\Psi(x) = \Psi_0 e^{-\lambda x}. \tag{12}$$

We will refer to λ^{-1} as the width of the current. This profile is also convenient because, having no inflection point in the vorticity, it is barotropically stable. The velocity $V = -\lambda\Psi$ and vorticity $\omega = \lambda^2\Psi$ of the coastal jet are greatest in magnitude on the coast. This profile is only possible when the coast is modeled as a slip boundary. Such boundary conditions are often used when the details of the coastal region cannot be resolved and when it is reasonable to model the large-scale motions as a flow slipping past the coast on a buffer zone that effects that actual transition of the flow to the no-slip shore (cf. Pond and Pickard 1978; Pedlosky 1996).

The exponential profile implies that F is linear. From Eq. (11) we have

$$F(\Psi) = \lambda^2\Psi. \tag{13}$$

Using this function F in the governing equation (8) for the topographic response leads to

$$(\nabla^2 - \lambda^2)\varphi = -h. \tag{14}$$

Thus, we arrive at an inhomogeneous Helmholtz equation for the response φ. In addition to the vanishing of φ for $y \to -\infty$, we also demand that it vanish on the coast ($x = 0$) so that there is no flow through the coast.

It is worth emphasizing that the sum $\psi = \Psi + \varphi$ is an *exact* solution of the fully nonlinear equation of mo-

tion (3). It is interesting that the topographic response satisfies a linear inhomogeneous equation. Hence, φ is proportional to the topography, but can be of any amplitude compared to the coastal jet.

The solution for φ will be determined by a Green function approach. The Green function for the Helmholtz operator $(\nabla^2 - \lambda^2)$ on an infinite plane is $G(\mathbf{r}, \mathbf{r}') = -(1/2\pi)K_0(|\mathbf{r} - \mathbf{r}'|)$, where $\mathbf{r} = (x, y)$ and K_0 is the modified Bessel function of order 0. To meet the condition of no flow through the coastal boundary, one can add to this free-space Green function another with its singularity placed to the left of the coastline such that the combination vanishes when $x = x'$. Thus the half-plane Green function is

$$G(\mathbf{r}, \mathbf{r}') = -\frac{1}{2\pi}[K_0(|\mathbf{r} - \mathbf{r}'|) - K_0(|\mathbf{r} - \mathbf{r}''|)], \quad (15)$$

where $\mathbf{r}'' = (-x', y')$. Then the formal solution to (14) is

$$\varphi = -\iint dx'\, dy' G(\mathbf{r}, \mathbf{r}')h(y'), \quad (16)$$

where the minus sign arises since the forcing in (14) is $-h$. The form of the Green function used here makes it difficult to exploit the fact that h is independent of x. After performing the x' integral in (16) and following a tedious series of nonobvious transformations, a much simpler Green function with no dependence on x' can be obtained. Rather than pursue this route, we will present a much simpler derivation of the result.

To find a simpler representation of the Green function, we solve for the reduced Green function $g(x, y - y')$ directly by solving

$$(\nabla^2 - \lambda^2)g(x, y - y') = \delta(y - y'), \quad (17)$$

where $\delta(y - y')$ is the Dirac delta function (cf. Gel'fand and Shilov 1964). Once g is obtained, φ will be expressible as a one-dimensional integral:

$$\varphi = -g * h \equiv -\int_{-\infty}^{\infty} g(x, y - y')h(y')\, dy'. \quad (18)$$

Note that we use an asterisk to represent convolution. To solve (17), we first Fourier transform in y, which leads to

$$\tilde{g}_{xx} - (l^2 + \lambda^2)\tilde{g} = 1. \quad (19)$$

The general solution to this equation is

$$\tilde{g} = -\frac{1}{l^2 + \lambda^2} + Ae^{-(l^2+\lambda^2)^{1/2}x} + Be^{+(l^2+\lambda^2)^{1/2}x}. \quad (20)$$

Demanding that g remains bounded as $x \to \infty$ and that $g(0, y - y') = 0$, so that φ will satisfy the appropriate boundary conditions, then leads to

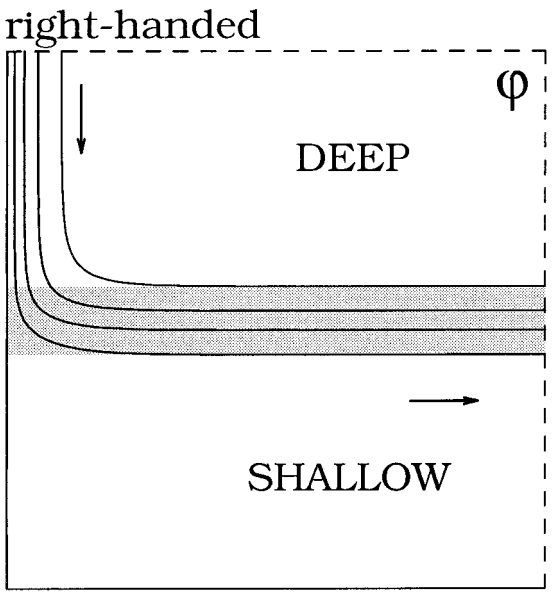

FIG. 2. Contour plot of the topography-induced streamfunction φ given by (18) and (22) for the particular form of topography given in (23). The contour interval is $0.2|h_0/\lambda^2|$. The arrows indicate the direction of the current represented by φ. Gray shading represents the region of the slope of width w. Here $\lambda^{-1} = 0.5w$.

$$\tilde{g} = \left[\frac{e^{-(l^2+\lambda^2)^{1/2}x} - 1}{l^2 + \lambda^2}\right], \quad (21)$$

$$g(x, y) = -\frac{1}{\pi\lambda}\int_1^{\infty} \sin(\lambda x[v^2 - 1]^{1/2})\frac{e^{-\lambda v|y|}}{v^2 - 1}\, dv, \quad (22)$$

The details of the calculation are presented in the appendix. This approach was also taken by E. R. Johnson (1978, unpublished manuscript).

It is clear from (22) that the Green function for the problem is symmetric in y, as might be expected. In essence, the Green function does not contain information about the form of the topography. With this Green function, the upstream boundary condition that we used on the topography, $h(x, -\infty) = 0$, guarantees the vanishing of $\varphi(x, -\infty)$. This, of course, can be changed if we want the unperturbed current to flow in the opposite direction, that is, if we have the inlet condition at $y = +\infty$. This change of boundary condition is simply accomplished by adding a dynamically insignificant constant to h so that $h(x, \infty) = 0$ and then we would have $\varphi(x, \infty) = 0$.

An example of the solution $\varphi(x, y)$ for the inlet conditions at $y = -\infty$ is shown in Fig. 2. Here we have taken a particular form of h given in terms of a stretched coordinate η by

$$h = \begin{cases} h_0 & \text{if } \eta > 1 \\ h_0(3\eta^2 - 2\eta^3) & \text{if } 0 \le \eta \le 1 \\ 0 & \text{if } \eta < 0, \end{cases} \quad (23)$$

where $\eta = (y + w/2)/w$ in which w is the width of the

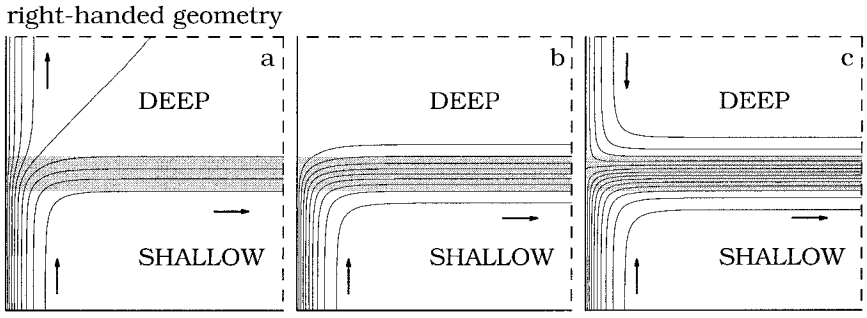

FIG. 3. Full solution $\psi = \Psi + \varphi$ for three different levels of the topography: (a) $h_0/|\omega_0| = -1/2$, (b) $h_0/|\omega_0| = -1$, and (c) $h_0/|\omega_0| = -1.5$. The contour interval is $0.2|\omega_0/\lambda^2|$ and $\lambda^{-1} = 0.5w$. Gray shading represents the region of the slope.

step. This represents a smooth transition from the shallow to deep fluid. The slope is nearly constant except near the end points at $y = \pm w/2$ where the profile curves so that the derivative of the topography, as well as the topography itself, is continuous. Up to an additive constant, $h(y)$ is antisymmetric in y, and hence its derivative is symmetric in y. For the case that leads to Fig. 2, h_0 is chosen negative to give the right-handed geometry. Note that φ then corresponds to a flow that comes from $y \to +\infty$ and then flows out along the step. The strength of the flow represented by φ is proportional to h_0. In the figure, we have indicated the open boundaries by dashed lines. The coast, where $\varphi = 0$, is drawn as a solid line. We indicate that $\varphi \to 0$ for $y \to -\infty$ is specified by drawing the bottom boundary also as a solid line.

The full solution, including the imposed coastal current, can now be represented. Clearly from Eq. (12), the direction of the coastal current depends on the sign of Ψ. To begin, let us assume the the imposed boundary condition at $y \to -\infty$ corresponds to an inflow of current; that is, we take $\Psi_0 < 0$. Thus the current is a negative vorticity current. It is convenient to represent the topographic amplitude h_0 in units of the maximum vorticity magnitude, $|\omega_0| = |\lambda^2\Psi_0|$, of the unperturbed flow. In Fig. 3, we show the full solutions $\psi = \Psi + \varphi$ for three representative topographic amplitudes in the right-handed geometry: (a) $h_0/|\omega_0| = -\frac{1}{2}$, (b) $h_0/|\omega_0| = -1$, and (c) $h_0/|\omega_0| = -1.5$. Note that negative values for h_0 imply that the fluid is shallow in the lower and deep in the upper portion of each figure. If $|h_0/\omega_0| < 1$, the coastal current bifurcates, with one branch continuing along the coast and the other flowing away from the shore along the topographic step. This is shown in Fig. 3a. If the topographic magnitude $|h_0|$ is increased, then the response can become strong enough to completely cancel the downstream flow, and the full solution shows the coastal current diverted entirely along the topographic step. This occurs for the critical value $h_0/|\omega_0| = -1$ (see Fig. 3b). If the size of the topographic step is increased beyond this critical value, then the coastal flow in the upper portion of the figure actually reverses. There is then an inward flow along the coast from $y = +\infty$ to meet the unperturbed coastal current at the step, and then the two coastal currents flow together away from the shore, along the step (see Fig. 3c). Hence, there is a stagnation point on the coast in the flow for $h_0/|\omega_0| < -1$ (see Fig. 3c). The existence of this stagnation point may be understood in terms of vorticity dynamics. If the topographic contribution to potential vorticity beyond the escarpment is greater than the relative vorticity of the incoming jet, then, as the jet crosses the escarpment, the sign of its relative vorticity reverses and subsequently the direction of the coastal flow reverses. The position of the stagnation point depends on the value of $h_0/|\omega_0|$ and varies from $y = -\infty$ to $y = +\infty$ as $h_0/|\omega_0|$ varies from $-\infty$ to -1. A graph of the behavior of the position of the stagnation point as a function of $h_0/|\omega_0|$ is shown in Fig. 4. This reversal of the current is possible because the boundary condition at $y \to +\infty$ was left open in our formulation.

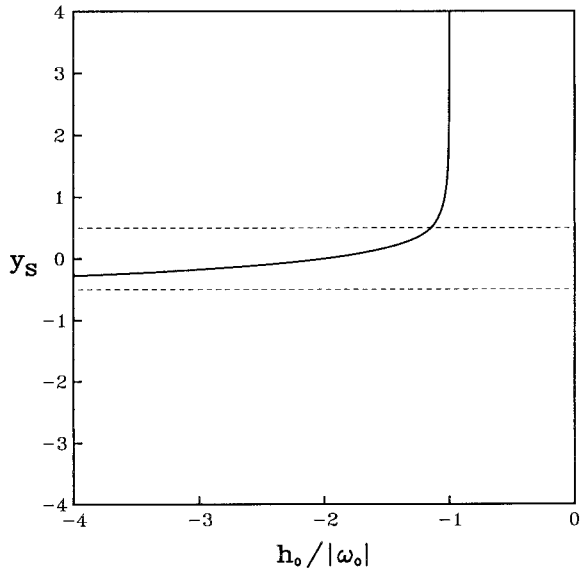

FIG. 4. Graph of the value of the stagnation point as a function of $h_0/|\omega_0|$; y_S is measured in units of w, the width of the topography.

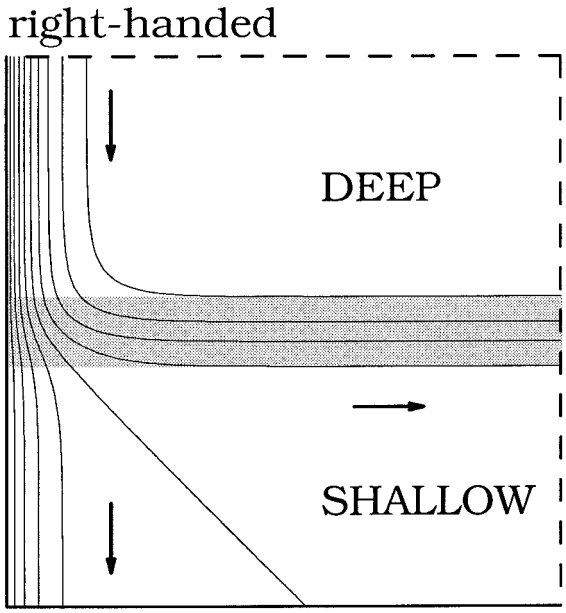

FIG. 5. Contour plot of the full solution $\psi = \Psi + \varphi$ with outflow on the bottom boundary for the topography such that $h_0/|\omega_0| = -1/2$. The contour interval is $0.1|\omega_0/\lambda^2|$. Gray shading represents the region of the slope.

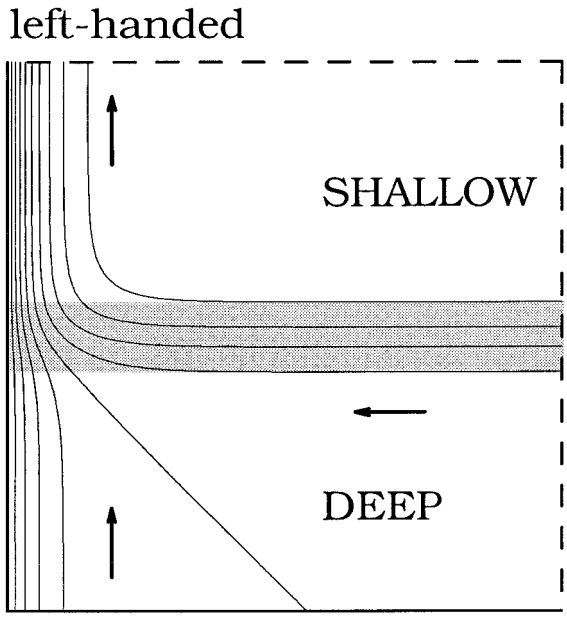

FIG. 6. Contour plot of the full solution $\psi = \Psi + \varphi$ for the topography such that $h_0/|\omega_0| = 1/2$. The contour interval is $0.1|\omega_0/\lambda^2|$. Gray shading represents the region of the slope.

By setting the relation F between streamfunction and potential vorticity to be the same everywhere, we have induced a strong inflowing current from the downstream boundary when h_0 is sufficiently negative. If we want to impose a ''downstream'' condition that does not allow such inflow, we would need to introduce different values of F in different regions as discussed below, and then the problem becomes analytically intractable.

The solutions discussed so far were constrained by the requirement that we specify the coastal flow at $y = -\infty$ as an *inflow*. If we relax this condition and change the sign of Ψ_0, thus specifying an *outflow* at $y = -\infty$, then additional solutions are possible. For the right-handed geometry, the form of these solutions is always as shown in Fig. 5, independent of the magnitude of h_0. This is because the perturbation φ (see Fig. 2) has a flow in the same direction as the unperturbed current along the coast. Thus we cannot reverse the direction of the coastal current by changing the magnitude of h_0 in this case.

Next we shall consider the solutions in the left-handed geometry. The forms of these solutions can be obtained directly from the solutions given above for the right-handed geometry by a simple symmetry transformation. From (7), we see that for every solution ψ with given topography h, we have the corresponding solution defined by the transformation $\psi(x, y) \to -\psi(x, y)$ and $h(y) \to -h(y)$. Thus, for example, this transformation applied to the case shown in Fig. 5 for flow in the right-handed geometry with *outflow* specified at $y = -\infty$ produces the result shown in Fig. 6 for flow in the left-handed geometry with *inflow* specified at $y = -\infty$.

Similarly, all of the right-handed geometry solutions shown in Fig. 3 have their counterparts in the left-handed geometry as shown in Fig. 7. The solid line on the bottom of the diagrams now indicates the boundary where the outflow is the prescribed exponential function.

The remarkable thing about the solutions for the left-handed geometry is that the flow along the step is always toward the coast. The steady coastal current across the step in the left-handed geometry does not bifurcate, but rather is joined by an inshore current flowing along the step, which reinforces the coastal current—in the case in Figs. 7b,c the step current is the source for the entire coastal current. Thus, as long as the relationship between streamfunction and potential vorticity is set at the the boundary at $y \to -\infty$, there is only one stationary flow, and it has this feature of inflow along the step.

We can see how the handedness of the geometry determines the direction of the flow along the step in our solution by examining the far field ($x \to \infty$). The behavior of (22) for large x may be found after making the change of variable $s^2 = v^2 - 1$. Then

$$\varphi = \frac{1}{\pi\lambda} \int_0^\infty \frac{\sin(\lambda x s)}{s} \frac{h^* e^{-\lambda(1+s^2)^{1/2}|y|}}{(1 + s^2)^{1/2}}\, ds. \qquad (24)$$

Note that

$$\lim_{x\to\infty} \frac{\sin(\lambda x s)}{s} = \pi\delta(s), \qquad (25)$$

where $\delta(\ )$ is the Dirac delta function (cf. Messiah 1961). Thus, in the limit $x \to \infty$, we have

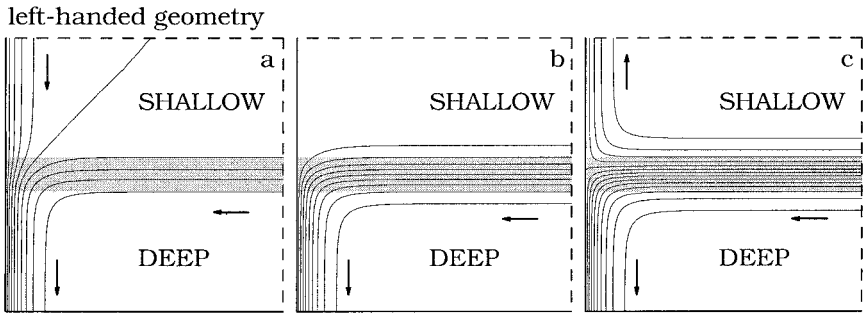

FIG. 7. Full solution $\psi = \Psi + \varphi$, with outflow specified at $y \to -\infty$, for three different levels of the topography: (a) $h_0/|\omega_0| = 1/2$, (b) $h_0/|\omega_0| = 1$, and (c) $h_0/|\omega_0| = 1.5$. The contour interval $0.2|\omega_0/\lambda^2|$. Gray shading represents the region of the slope.

$$\varphi = \frac{h * e^{-\lambda|y|}}{2\lambda}, \tag{26}$$

where the factor of ½ arises from the fact that the integral terminates at $s = 0$. This is exactly the solution to the one-dimensional problem,

$$\varphi_{yy} - \lambda^2\varphi + h = 0, \tag{27}$$

which is what would be expected from Eq. (14) at large distances x where the x dependence vanishes.

Since there is no x variation in the far field result (26), for large x the velocity is directed only along the step and is given by

$$u = -\frac{e^{-\lambda|y|}}{2\lambda} * h'(y). \tag{28}$$

The right-handed geometry (with the wall on the left) has $h'(y) < 0$, so the flow far from the coast will be directed away from the shore. For the left-handed geometry, $h'(y) > 0$, and the flow will be toward the coast. Furthermore, from Eq. (27), it follows that for large x and large $|y|$ we have $\varphi = h/\lambda^2$. Thus, the total mass flux leaving the domain along the step is

$$\int_{-\infty}^{+\infty} u\, dy = -(\varphi(+\infty) - \varphi(-\infty)) = -\frac{h_0}{\lambda^2}. \tag{29}$$

Note that this is independent of the mass flux entering the domain with the inlet coastal current. Any difference between the two is compensated by the flow through the top boundary (i.e., $y = +\infty$).

Up to this point, we have been displaying only solutions for the case with the unperturbed coastal flow specified at $y = -\infty$. What happens if the unperturbed coastal current is specified at $y = +\infty$? The result can be deduced from the solutions given above and symmetry considerations. Let us assume that the topography, save perhaps for an additive constant, is antisymmetric in y, which means that the gradient of the topography is symmetric in y. Consequently, if we have a solution to the stationary state equation (7) given by $\psi = \Psi(x) + \varphi(x, y)$, then $\psi = -\Psi(x) - \varphi(x, -y)$ is also a solution, as can be seen by substituting this form for ψ in the Jacobian, $J(\psi, \nabla^2\psi + h)$. Exploiting the symmetry of $\partial h/\partial y$ and making the change of variables $y \to -y$ then shows that the Jacobian must vanish. Thus, for the given topography, the form of the streamfunctions will not change under coastal current reversal save for this simple symmetry transformation. This is illustrated for the right-handed geometry in Fig. 8. Note that in Fig. 8b the inflow boundary condition is specified on the top boundary as indicated by the solid line. In both cases shown, with the coastal flow encountering either a step up or step down, the flow along the step is directed offshore. Similarly, if we consider the left-handed geometry, we find that the topographic current is toward the coast irrespective of whether the coastal flow encounters a step up or step down. It is the handedness of the geometry that determines the direction of the current on the step and not the direction of the coastal current.

We must end this section with a note of caution. The solution obtained here is not unique. Even assuming the specific exponential inflow boundary condition as we did, there is still an element of ambiguity introduced by the lack of explicit boundary conditions on the downstream and offshore boundaries. For example, we could specify the downstream boundary with an inflow velocity profile rather different from that found in our analytic solution. This would necessitate introducing an-

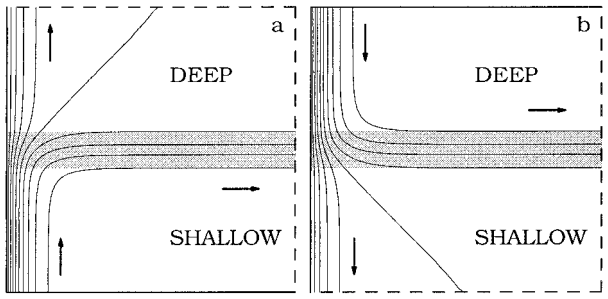

FIG. 8. Stationary streamfunction in the right-handed geometry for $|h_0/\omega_0| = 0.5$ for (a) step-down configuration and (b) step-up configuration. The contour interval is $0.1|h_0/\lambda^2|$. Gray shading represents the position of the slope.

other form for F in the region of that boundary. We can in general imagine the function F specified differently in different regions of the flow. The values of F in each region would be determined by the relation between streamfunction and potential vorticity on the adjacent external boundaries through which streamlines pass. Boundaries between different regions of F in the interior of the flow are acceptable as long as those boundaries are streamlines. In fact, wholly interior regions with an arbitrary specification of F would also be possible as long as there is no exchange of fluid with such a region and the surrounding flow. The appropriate choice of boundary conditions will depend on the specific nature of the problem under consideration. Here the flows on the originally unspecified boundaries are determined by our demand that F be the same function everywhere. Thus, we must expect that the analytic solution will be valid everywhere only when all of the streamlines in the flow intersect the boundary where we have specified the relation between streamfunction and potential vorticity (i.e., in the cases for which $|h_0/\omega_0| < 1$).

3. Numerical simulations

We have performed a series of numerical simulations of the quasigeostrophic flow over a step. The geometry for the numerical simulations is the same as that considered above with the step profile given by (23). Here our main interest is to gain insight into the dynamics of the interaction of the coastal flow with the step. The boundary conditions, as described below, are designed to focus attention on the dynamics of the interaction rather than to reproduce our analytic solution.

We begin the simulations from a state of no motion and introduce a coastal flow at one boundary. The flow through this inlet boundary is smoothly increased during a period of two advective time units to the steady state exponential velocity profile given in (12). We define the advective time unit as $1/\omega_0$, or equivalently $1/(\lambda V_0)$, where V_0 is the maximum velocity and λ^{-1} is the width of the coastal unperturbed steady current. The inlet boundary is taken sufficiently far from the topography so as to minimize the effects of the finite size computational domain.

Since we are mainly concerned with understanding the results of the interaction of our coastal current and the topography, we have used a radiation boundary condition on the open ocean and the downstream boundaries. This is the choice that best represents the dynamics of the interaction between the approaching coastal current and the escarpment on a semi-infinite domain. These boundary conditions will minimize the effects of the geometry of the computational boundaries other than that of the coast. However, the downstream and offshore boundary conditions of the simulation differ from the analytical steady-state solution in cases that require specification of inflow on offshore and downstream boundaries because the flow on the radiation boundaries can only evolve due to the influence of the vorticity field within the computational domain. For the radiation condition we use the Orlanski (1976) algorithm. In this method the boundary conditions for ψ and ω are changed each time step according to an estimate of the rate of change of these quantities near the boundary from previous time steps.

For the coastal boundary, we use a slip boundary condition. For the streamfunction this simply means that we impose that ψ is a fixed constant on the wall, which implies no normal flow. The presence of Laplacian diffusion in our code raises a complication, however. Unfortunately this diffusion cannot be set equal to zero in this finite difference code without losing numerical stability. With finite viscosity, we will also need to specify the vorticity at the slip wall. The typical stress-free boundary conditions on a straight boundary would require that we set $\omega = 0$. This, however, is inappropriate for the present problem for two reasons. One is that the coastal current that we want to model has maximum vorticity at the wall. The second, and perhaps more important reason, is that as a fluid particle moving along the boundary encounters the topography its relative vorticity must change by vortex stretching. Similar dilemmas have been faced in other applications as discussed by Roache (1972). The remedy that seems best for the present problem is to take the values of ω on the wall to be identical to those just off the wall. Thus as the nearby particles adjust to changes in topography, the same adjustment is forced at the wall. Thus, we have imposed $\partial\omega/\partial n = 0$ at the wall where n is the coordinate in the direction normal to the wall. This boundary condition is sometimes referred to as ''superslip'' (cf. Pedlosky 1996).

The time stepping in these simulations is Runge–Kutta third order, which is optimal for efficient memory usage (Rai and Moin 1991) and permits a fairly large time step. The size of the time step is adjusted after each step according to the conditions of the CFL criterion (cf. Peyret and Taylor 1983) permitting high efficiency.

As a first example, we consider the case of the right-handed geometry with an inlet condition such that $h_0/|\omega_0| = -0.5$. In this case, the analytic theory predicts that in the steady state the coastal current bifurcates with one branch following the coast and the other flowing outward along the step. We began by simulating the evolution of the flow from rest until a stationary state was reached at Reynolds number 750 defined by $\mathrm{Re} = V_0\lambda^{-1}/\nu$. This stationary state was close to the theoretical prediction, but the results were improved somewhat by continuing the evolution at Reynolds number 2500. The result for this high Reynolds number, long-term evolution is shown in Fig. 9. In panel (a) we show the streamfunction from the simulation (solid contours) superimposed on the theoretical streamfunction (dotted contours). The resulting match is nearly perfect. The one contour that does not match well is in a region of

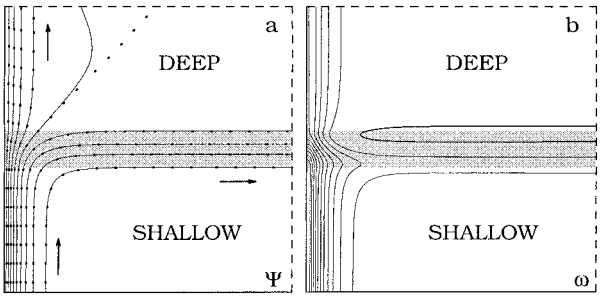

FIG. 9. Contour plots of the stationary flow in the right-handed geometry for the case $h_0/|\omega_0| = -½$, at Reynolds number 2500, in the step-up configuration. (a) Contours of the streamfunction from the simulation (solid curves) and the theory (dots). The contour interval is $0.1|\omega_0/\lambda^2|$. (b) Contours of relative vorticity. Thin (thick) lines represent levels of negative (positive) vorticity. The contour interval is $0.075|\omega_0|$. The zero vorticity isolevel is not drawn.

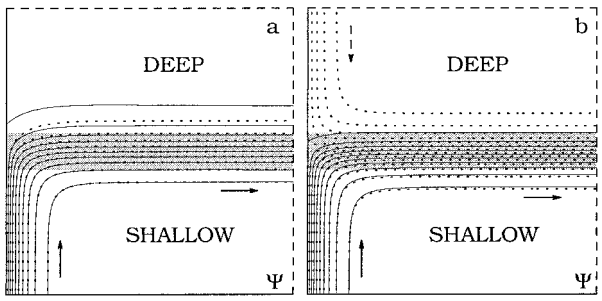

FIG. 10. Contour plots of the streamfunction for the stationary flow in the right-handed geometry at Reynolds number 2500, in the step-up configuration. Contours of the streamfunction from the simulation are shown as solid curves while the dashed curves indicate the theoretical prediction. (a) Case $h_0/|\omega_0| = -1$. (b) Case $h_0/|\omega_0| = -1.5$. (Contour level increment = $|\omega_0/\lambda^2|$.)

very slow flow and is slowly evolving toward the stationary state result. In panel (b) we show the relative vorticity distribution in the simulated flow. The vorticity in the coastal current is all negative. Note that over the topography there is both positive and negative vorticity, with the positive vorticity to the left of the negative looking out from the coast, as is necessary to have a jet away from the coast (cf. Stern and Austin 1995). The positive vorticity is created by the advection of fluid from shallower levels to deeper levels. The stretching of the fluid columns creates the positive relative vorticity in accordance with the conservation law of potential vorticity. This simulation corresponds to the step-down case. If we change the direction of the coastal current, then the final vorticity is given by the reflection and change of sign according to the discussion of the previous section. Thus, in going from the step-down to the step-up case we would have $\omega(x, y) \rightarrow -\omega(x, -y)$. In the step-up case, the coastal current would be all positive vorticity. Along the step, there would again be positive vorticity to the left of negative vorticity on the topography looking out from the coast. In this case the negative vorticity is created by fluid columns that have moved from deeper levels to shallower levels. The important thing is that, with this orientation of the positive and negative vorticity above the topography, the flow is again away from the coast.

It is not surprising that the numerical simulation can reach the stationary state predicted by our analytic solution for $h_0/|\omega_0| = -½$ because in this case all streamlines do pass through the boundary at $y = -\infty$, and hence the functional relationship between streamfunction and potential vorticity is the same throughout the domain. For larger topographic variations where the coastal current reverses in the analytic solution this will not be the case. In Fig. 10, we show the results for cases in which the theory predicts that the coastal current is totally blocked from proceeding along the coast. These are the cases for which $|h_0/\omega_0| \geq 1$. The match with the analytic solution (dashed lines) becomes less good as the strength of the topography increases due to the different downstream and offshore boundary conditions as discussed above. One could, of course, introduce additional inlet conditions on the downstream and offshore boundaries of the numerical simulation to simulate the conditions of the analytical problem that we solved, but prescribing the boundaries like that increases the importance of the boundary influence in the interaction while we prefer to focus on the interaction between a single coastal current and the escarpment.

Now we turn to the question of how the interaction between the coastal current and the topography establishes the current along the topography. In Fig. 11, we show the evolution of the vorticity field in the case of $|h_0/\omega_0| = 0.5$, in which the flow bifurcates. We have changed the orientation of the plots somewhat to facilitate comparison with the figures from the laboratory experiments shown in Stern and Austin (1995). The coastal flow now experiences a step down in crossing the step, but the dynamically relevant factor is that this is right-handed geometry.

A freely flowing coastal jet (with single signed vorticity) when started from a state of no flow, proceeds along the coast as a bulbous nose with a smooth uniform current following behind (cf. Stern and Whitehead 1990). In Fig. 11a, we see the early stage of the interaction of the nose of the current with the topography. In this step-up example of the coastal current in right-handed geometry, the vorticity in the coastal current is positive. Before the current reaches the topography, it pushes some of the zero-relative vorticity fluid that lies ahead of the nose uphill. By conservation of potential vorticity, this fluid must develop negative relative vorticity, and this is seen over the topography near the nose of the coastal current in panel (a). Also, as the current itself climbs the topography, the vorticity in the nose decreases by the compression of the fluid column. The net result is a strong negative vorticity anomaly, relative to the unperturbed case, which advects a portion of the coastal current vorticity away form the main current as shown in panel (b). The original negative vorticity patch

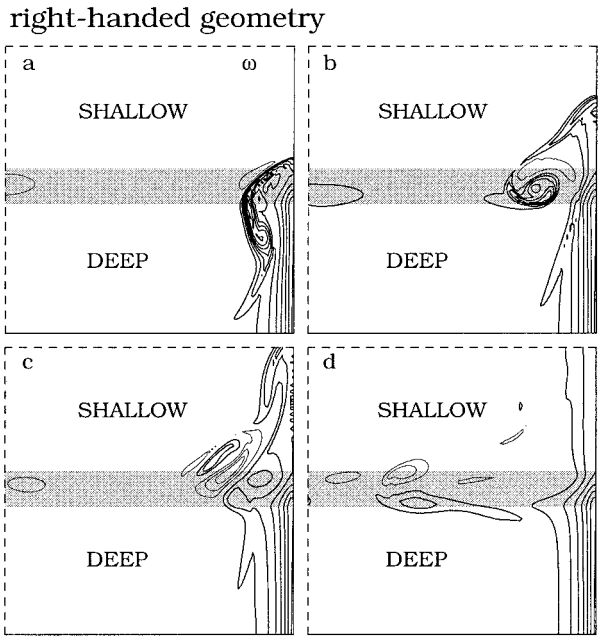

FIG. 11. Evolution of the vorticity field in a simulation of the flow of a coastal jet over a step in the right-handed geometry, with Re = 1500, in the step-down configuration. Positive (negative) levels of vorticity are indicated by thick (thin) lines. The zero vorticity contour level is not drawn. The contour interval is $\omega_0/8$. The gray shading indicates the topographic slope. The times represented by the panels are (a) 26, (b) 38, (c) 54, and (d) $116\omega_0^{-1}$. The ratio $|h_0/\omega_0|$ is 0.5, and $w = 2\lambda^{-1}$.

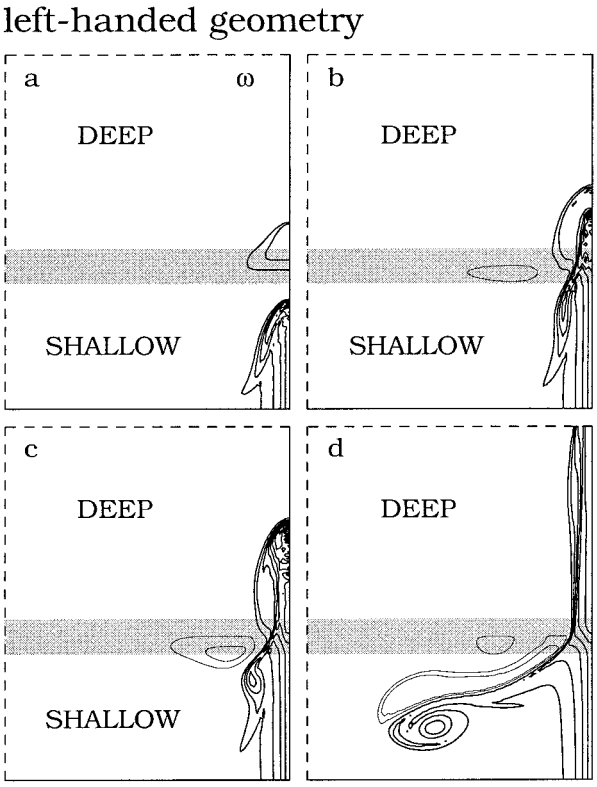

FIG. 12. Evolution of the vorticity field in a simulation of the flow of a costal jet over a step in the left-handed geometry, with Re = 1500, in the step-down configuration. Positive (negative) levels of vorticity are indicated by thick (thin) lines. The contour interval is $\omega_0/8$. The gray shading indicates the topographic slope. The times represented by the panels are (a) 7, (b) 22, (c) 28, and (d) $64\omega_0^{-1}$. The ratio $|h_0/\omega_0|$ is 0.5, and the step width is $w = 2\lambda^{-1}$.

pointed out in panel (a) is no longer observed in panel (b) because it has weakened due to the effects of viscous dissipation and no longer reaches the first contour interval plotted. In panel (b), there is a new patch of negative relative vorticity next to the cyclone that broke off the main current. This negative relative vorticity was formed because the cyclone, by advecting fluid counterclockwise, pulled low relative vorticity fluid uphill, thereby creating the anticyclonic vorticity. Then the cyclone pulls more fluid uphill creating yet another anticyclone, which is seen in panel (c). This anticyclone then induces the separation of yet another cyclone from the coastal current, and this one is stronger than the last. This new cyclone then in turn forms yet another anticyclone. This last pair of oppositely signed vortices dominates, forming a dipole that is sufficiently strong to propagate away from the coast. As this dipole propagates along the step (and eventually leaves the domain through the radiation condition wall), it leaves behind in its wake the positive and negative vorticity that eventually forms the stable stationary current along the topography of Fig. 9b. The details of the multiple vortex generation vary depending on the topographic profile and the Reynolds number, but the important thing is that a strong dipolar vortex eventually forms and moves along the step with a branch of the bifurcated jet following behind.

Given the differences in the direction of topographic wave propagation as discussed in the introduction, and the differences in the analytic solutions as discussed in the last section, we would expect that the evolution of the flow in the left-handed geometry is very different from that in the right-handed geometry. The evolution of the relative vorticity field for the left-handed case is shown in Fig. 12. Instead of a dipole that moves along the step, in this case a dipole is formed that moves off the step. Let us examine the stages of this dipole formation. The process is much simpler than that in the right-handed geometry. The early stage is shown in panel (a). As the coastal current approaches the step, some fluid ahead of the jet is forced to move downslope, thus creating the separate cyclone seen over the slope. In panel (b), the coastal current catches up with and merges with the cyclone that was lying over the slope. As the nose of this cyclonic jet passes the step, it induces fluid on the step to move around it in a counterclockwise arc, which takes *it* upslope. This fluid moving upslope must acquire negative relative vorticity creating an anticyclone. This anticyclone strengthens as it moves farther upslope. In panel (c) we see that it is strong enough to induce the roll-up of part of the coastal jet, which forms

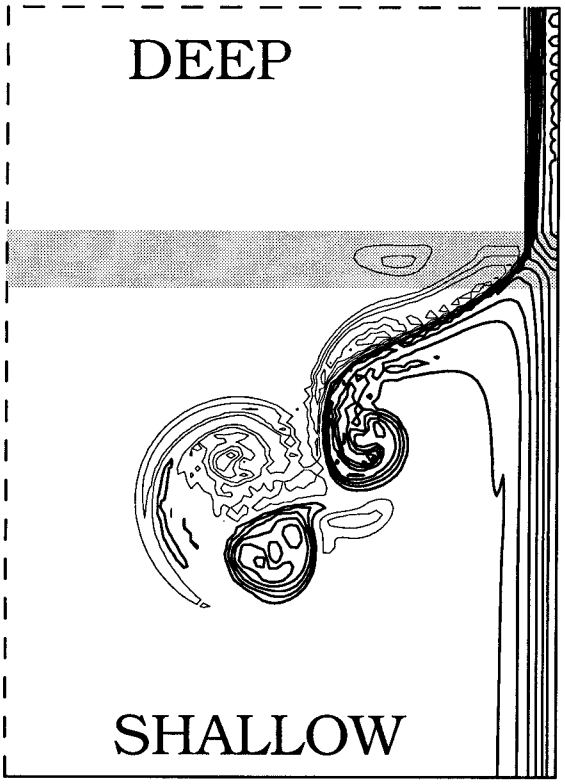

FIG. 13. Vorticity field from a simulation of the flow of a costal jet over a step in the left-handed geometry with slope and width as in Fig. 11 but at a later time ($t = 120\omega_0^{-1}$) showing the formation of a secondary dipole. Positive (negative) levels of vorticity are indicated by thick (thin) lines. The contour interval is $\omega_0/4$. The gray shading indicates the topographic slope. The computational domain was 20×40 in units of λ^{-1}, but here we have zoomed in on an area of size 20×28.

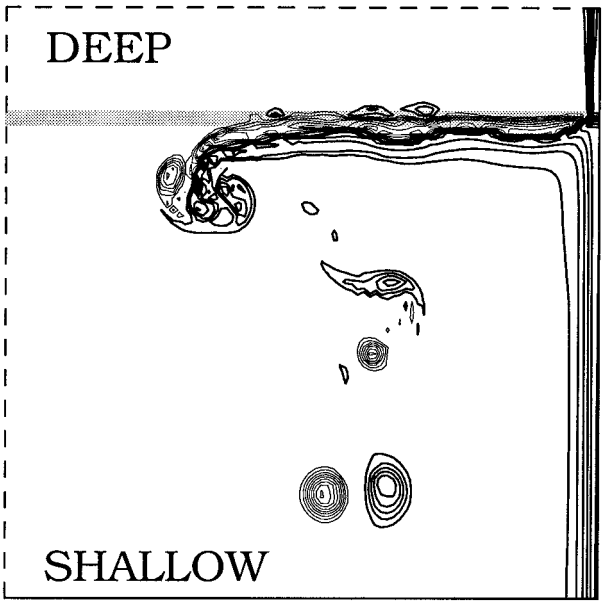

FIG. 14. Vorticity field from a simulation of the flow of a costal jet over a step in the left-handed geometry. By $t = 220\omega_0^{-1}$ three dipoles have formed and left the slope. Note that the point of separation from the slope is far from the coast in contrast to the case shown in Fig. 13. Positive (negative) levels of vorticity are indicated by thick (thin) lines. The contour interval is $\omega_0/8$. The gray shading indicates the topographic slope. The ratio $|h_0/\omega_0|$ is 1 and the step width is $w = \lambda^{-1}$. Domain size is $40\lambda^{-1}$ in both the x and y directions.

a cyclone. The resultant cyclone–anticyclone pair is oriented at an angle from the step and once created, there is nothing to prevent it from moving off in that direction [see panel (d)].

If we compare the evolution in the right-handed and left-handed geometries, we see the formation of a dipole in both cases. In the case of the right-handed geometry, the dipole could not move off the topography in the upstream ($-y$) direction because, once it left the topography, the anticyclone would lose all of its strength due to conservation of potential vorticity. In the left-handed geometry, in contrast, as the anticyclone moves in the upstream direction, it reaches its maximum strength as it comes off the slope. Thus, there is nothing to block the dipole in that case from moving off the topography in the upstream direction.

This formation of a dipole shown in Fig. 12 for the left-handed geometry is very similar to that observed in Stern and Austin (1995). Their experiments use a left-handed geometry. They suggested that the formation of the dipole moving off the topography had to do with the dissipative effects of the bottom Ekman layer in the tank. The simulation shown in Fig. 12 demonstrates that this result does not require an Ekman boundary layer.

If we run simulations in the left-handed geometry for longer periods of time, the dipole production repeats itself. For example, in Fig. 13 we show the results of a simulation run with the same topography and boundary current as used in the simulation shown in Fig. 12. Here we have allowed the simulation to run longer, illustrating the formation of a second dipole (the domain size was doubled in the y direction to allow more space for the continued evolution).

To see how the results shown above depend on the choice of slope and width of the topography, we performed a series of simulations in which $|h_0/\omega_0|$ was varied from 0.25 to 8 and the width of the topography was varied from 0.5 to 4 λ^{-1}. We found that the position of the initial dipole and the angle at which it left the slope were not very sensitive to the changes in the topographic width. However, the position where the dipole left the slope could be moved farther from the coast by making the depth variation greater. For example, in Fig. 14, we show a case where $|h_0/\omega_0| = 1$. The dipoles are now shed from the slope at a position which is many coastal-current widths from the coast.

That the position at which the dipole leaves the topography can be moved farther offshore raises an interesting possibility. By making the depth variation

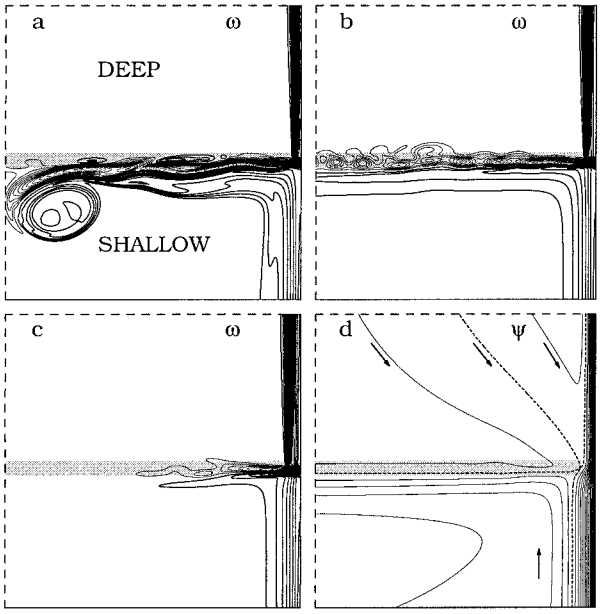

FIG. 15. Vorticity and streamfunction fields from a simulation of the flow of a costal jet over a step in the left-handed geometry. Positive (negative) levels of vorticity are indicated by thick (thin) lines. The dashed lines indicate the streamlines connected to the saddle point as discussed in the text. The gray shading indicates the topographic slope. The ratio $|h_0/\omega_0|$ is 2, the step width is $w = \lambda^{-1}$, and Re = 750. The computational domain size in the x direction was $10\lambda^{-1}$ and in the y direction it was $20\lambda^{-1}$. In the y direction, only the region of size $10\lambda^{-1}$ centered on the topography is shown. The fields are (a) ω at $t = 100\omega_0^{-1}$, (b) ω at $t = 400\omega_0^{-1}$, (c) ω at $t = 2400\omega_0^{-1}$, and (d) ψ at $t = 2400\omega_0^{-1}$. The contour intervals are $0.1\omega_0$ for the vorticity and $0.5\omega_0\lambda^{-2}$ for the streamfunction.

strong enough so that any dipole shedding would occur outside of the computational domain should allow the establishment of steady-state offshore flow, even in the left-handed geometry. In Fig. 15, we provide an example of the formation of such a current. The topography is such that $|h_0/\omega_0| = 2$. This is sufficiently strong so that the dipole just begins to separate at the outer edge of the computational domain as is seen in Fig. 15a, which corresponds to $t = 100\omega_0^{-1}$. Shortly after the dipole begins to separate, it passes through the radiation-condition boundary. Over the topography, we are then left with an offshore current on which are superimposed negative relative vorticity fluctuations with horizontal scale similar to the width of the topography. These fluctuations are visible in Fig. 15b, which corresponds to $t = 400\omega_0^{-1}$. On a longer timescale, the viscous timescale, these fluctuations diffuse away to a certain extent. By time $t = 2400\omega_0^{-1}$, a steady state has been established (see Fig. 15c) in which some small-scale variation of the vorticity filed persists near the coast, but is not strongly evident in the streamfunction (see Fig. 15d). We simulated this flow out to time $t = 6400\omega_0^{-1}$ to confirm that it is indeed stationary and observed no further changes. The final streamfunction pattern is interesting. There is a saddle point in the field occurring over the topography and just outside the main coastal current. We have indicated the streamlines that connect to this saddle point by dashed lines. On the upstream side of the topography (small y), the dashed streamline divides the coastal current into two parts. The part closest to the wall is that which passes the topography and continues along the coast. This is about 80% of the total flow. The remainder follows the topography of the step, forming the main part of the offshore current. On the downstream side, the dashed lines break the flow into three parts. One part close to the wall is the current that continued along the coast after passing the step. Next to this is a region in which there is an inflow or backflow from the downstream boundary that turns around and joins the outgoing coastal current. This back flow is formed when the nose of the propagating coastal current passes through the downstream boundary. Also in the region farthest from the coast there is an inflow from the downstream boundary that joins the offshore current along the topography. This strengthens the offshore current by about 25%. None of these aspects of the stationary flow can be captured by the analytic inviscid solution presented above. Recall that in that solution the ratio between potential vorticity and streamfunction is constant throughout the domain, while in the flow shown in Fig. 15 that relationship is maintained only in the coastal current, and there only approximately because of the effects of viscosity. In the region of the back flow from the downstream boundary, the flow is approximately potential flow since there is a gradient of ψ but the vorticity is essentially zero.

Thus, it would appear that, in this simulation with the boundary conditions determined by the Orlanski condition, it is possible to obtain a stationary offshore current along the topography even in the left-handed geometry. The presence of the saddle point in the streamfunction and some of the small-scale vorticity variations near the coast make this flow rather different from the stationary flow in the right-hand geometry. It may be that stationary flows in the left-handed geometry are obtainable once the appropriate boundary conditions are applied even in the inviscid problem as suggested by the analysis in Spitz and Nof (1991) and Stern and Austin (1995). On the other hand, it may be that, at least with the initialization of the flow as in our simulations, nonzero viscosity is necessary to obtain steady flows. The Reynolds number for the flow shown in Fig. 15 is 750. We have compared this with a simulation at Reynolds number 375. In the latter case, the stationary flow appears similar to that in Fig. 15b, and there are stationary small-scale vorticity variations all along the topography. It seems that the higher viscosity stabilizes these variations. Perhaps they can exist in stationary form only with finite viscosity. Also, the time it takes to reach stationarity varies with the Reynolds number in a way that suggests viscosity is important in reaching these stationary states. Increasing the Reynolds number above 750, we find that the flow along the topography

weakens and there is an inflow from the offshore boundary on the upstream side of the topography extending over a large part of the boundary. This again suggests that the existence of the offshore current along the topography may be a result of viscous effects and would not occur in a truly inviscid evolution on a semi-infinite domain with the given initial conditions.

4. Discussion

In this section we will expand on some of the points raised above and consider the relevance of this work to actual coastal flows. Let us return first to the question of the role of topographic wave propagation in the evolution of coastal flow across an escarpment. In the introduction we noted the analogy between the β-plane and topography problems. Indeed the effects of β and a constant slope are equivalent in quasigeostrophic theory. In this analogy, high (low) latitudes would correspond to shallow (deep) regions. Indeed we can speak of topographic west (east) as the directions in which shallow water is on the right (left) for the local topographic variation. Thus a western boundary would correspond to left-handed geometry and an eastern boundary to right-handed geometry in our nomenclature. That the phase velocity of the Rossby waves is always westward immediately points to a major difference in the two geometries. The anisotropic dispersion relation for Rossby waves leads to very different reflections at western and eastern boundaries. As a result, as LeBlond and Mysak (1978) point out, western (eastern) boundaries can be thought of as sources (sinks) for small-scale variability. This is in accord with our results, which show that in the right-handed geometry the flow soon settles into a large-scale stationary flow along the ridge, while in the left-handed geometry small-scale variations in the vorticity field are maintained over the topography near the coast. Another point to make is that westward and eastward flow on a β plane are very different in terms of the waves produced by a localized disturbance. This is clearly seen in Thompson and Flierl (1993) where large-scale flow on a β plane over an isolated topographic feature is examined. Eastward flow over the obstacle produces strong wave activity downstream, while this does not occur for westward flow. Also, we can note that although stationary flow in either the westward or eastward direction is possible on the beta plane, only westward flow is predicted to be stable based on energy and enstrophy considerations (cf. Bretherton and Haidvogel 1976; Salmon et al. 1976; Carnevale and Frederiksen 1987; Holloway 1986).

Pursuing the wave ideas further, we consider a model in which we linearize about the state of no motion. Thus the evolution equation 3 becomes

$$\frac{\partial \omega}{\partial t} + \frac{\partial \psi}{\partial x}\frac{\partial h}{\partial y} = 0. \tag{30}$$

In this model, we would imagine any evolving flow to be composed of the free oscillations of this system. Then the stationary state would be achieved as all propagating modes radiate away leaving only the stationary (i.e., zero frequency) modes. This type of analysis has been used by several authors and yields many interesting results (cf. Longuet-Higgins 1968; Johnson 1985; and Willmott and Grimshaw 1991). But from (30) it is clear that the stationary modes must be such that ψ is independent of x for flow over the topography. However, such a stationary flow would be blocked by the coast and could not exist. This is evident in the solutions of Johnson (1985) and Willmot and Grimshaw (1991), which clearly show strong differences for right- and left-handed geometries; but the purely linear model does not show the kind of stationary currents exhibited above in the fully nonlinear model. To some extent, we can avoid this limitation of the linear model: if we realize that the coastal region can act as a forcing for Eq. (30), then we could add to this equation a forcing term on the right-hand side that is meant to account for the generation of waves due to the nonlinear interaction of the coastal current and the topography. Streamlines corresponding to a current along the topography can then be closed in the nonlinear coastal region. In such a model, we would expect, given the example of β-plane flow, that the forcing will radiate long wavelength waves that will settle down into a stationary current along the step in the right-handed geometry but a small-scale localized wave field in the left-handed geometry. To test this concept, we have performed simulations in which the flow within $2\lambda^{-1}$ of the coast is governed by the full nonlinear evolution Eq. (3), while for flow beyond this strip, the evolution is governed by the linear dynamics of equation (30). The hybrid evolution in the left-handed case shows an early phase in which waves with wavelength in the x direction comparable to λ^{-1} appear over the entire step slope. Gradually, the flow becomes limited to localized, growing, intense, small-scale variation in the vorticity shown in Fig. 16a. See Johnson and Davey (1990) for a purely linear treatment of this phenomenon. In contrast, in the right-handed geometry, the early evolution shows waves with somewhat longer wavelength and a tongue of the coastal current extending along the step. This slowly establishes an offshore current along the coast. In Fig. 16b we see the vorticity pattern of this current, which has reached a nearly steady state. Thus, even though the hybrid evolution cannot show the formation of the dipoles that are so dominating in the early evolution of the fully nonlinear simulations, the establishment of the current in the right-hand case is very similar to that in the nonlinear case.

Beyond the linear analysis given above, some useful insight can perhaps be gained by from a vortex stretching point of view as illustrated in the schematic shown in Fig. 17. In this figure we indicate the change in vorticity amplitude on crossing the step. For example, in panel (a) we consider the situation in the left-handed geometry for a current undergoing a step up. The an-

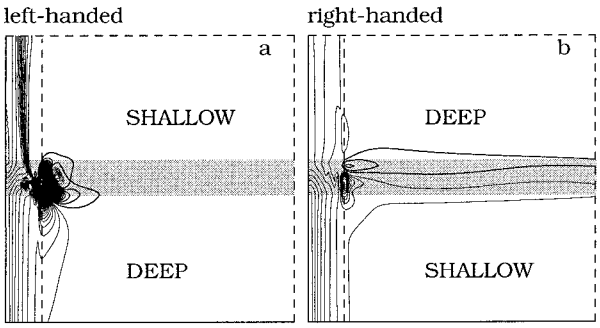

FIG. 16. Contour plots of relative vorticity in the hybrid simulation with fully nonlinear dynamics in the coastal region and purely linear dynamics outside that region. The width of the coastal region is taken as $2\lambda^{-1}$ and the full domain size is $8\lambda^{-1} \times 8\lambda^{-1}$. (a) Left-handed geometry and (b) right-handed geometry. The dividing line between the nonlinear and linear regions is indicated by the internal dashed line. The fields are shown at time $700\omega_0^{-1}$. The ''Reynolds number'' $V_0/\nu\lambda$ is set as 750 throughout the domain.

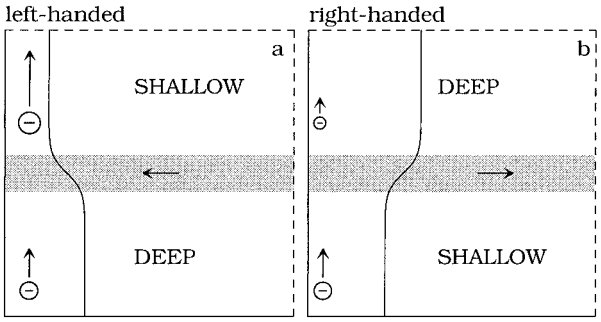

FIG. 17. Schematic showing the change in relative vorticity in the coastal current flowing over a step. The magnitude of the relative vorticity in an area is indicated by the size of the corresponding circle. (a) Left-handed geometry and (b) right-handed geometry. The limit of the current is indicated by a single streamline (solid curve).

ticyclonic vorticity in the boundary current must increase in strength when passing over the step to conserve potential vorticity. Since we are at a free-slip coast, we can think of the advection of the vorticity along the coast as a result of the flow field established by the vorticity in the coastal current and its ''image'' in the wall. In other words, the streamfunction in the interior in the presence of a wall can be obtained by calculating the streamfunction due to the actual vorticity and an image vorticity obtained by spatial reflection in the wall and a change of sign. The image vorticity also increases in magnitude when the real vorticity does. Thus the current accelerates. Recalling that quasigeostrophic flow is divergenceless, we see that the streamlines of the coastal current must then draw closer to the coast, that is the width of the current decreases. In the analytic solution this is accompanied by an influx of fluid along the step. If we reverse the direction of the coastal current, we then have the step-down case, but the results are the same. In that situation, the coastal current has positive relative vorticity, which on crossing the step will also strengthen; the flow again accelerates drawing the streamlines in toward the coast just as in the step-up case. Again, changing the direction of the current simply changes the sign of the vorticity, but the result is the same: the oncoming flow in the left-handed geometry is accelerated and its width decreases, whether going through a step-up or a step-down. In the right-handed case shown in panel (b), on crossing the step the negative vorticity is weakened by the step down. This decelerates the flow, pushing the streamline out and apparently also inducing an outward flow along the step. Again changing the direction of the current simply changes the sign of the vorticity, but the result is the same: the oncoming flow in the right-handed geometry is decelerated and its width increases, whether going through a step-up or a step-down. In the analytic solution this is accompanied by an outflow of fluid along the step. Allen and Hsieh (1997) give an interesting discussion of this flow deceleration in a two-layer shallow water model of flow past the Mendocino escarpment.

Another mode of investigating this problem has been through laboratory experiment. We have already discussed above the laboratory experiment of Stern and Austin (1995), which showed that, in the left-handed geometry, a coastal current impinging on a topographic step does not simply bifurcate but, rather, creates a dipole which moves off the step. We were able to capture this effect numerically as shown in Fig. 12. The stationary analytic solutions that we have presented and the arguments based on the direction of propagation of topographic Rossby waves suggest a priori that there should be a difference in such an experiment for left- and right-handed geometries. Spitz and Nof (1991) present experiments on coastal flow over a step for both right- and left-handed geometries. They consider a step-up flow in a right-handed geometry and a step-down flow in a left-handed geometry. Their laboratory set up involves a topographic step of infinite slope. The discontinuity in the topography takes the depth from 3 to 21 cm. Treating such a step is beyond the scope of the quasigeostrophic model. Nevertheless, we should make some comments on the Spitz and Nof (1991) experiments. Results from those experiments are shown in their Figs. 7 and 8. (Note that the figure captions for those figures have been interchanged.) Their Fig. 7 shows a step-up flow in a right-handed geometry and their Fig. 8 shows a step-down flow in a left-handed geometry. Both flows are blocked by the step, but there are differences in the right-handed and left-handed cases. In the right-handed case, the current flows out from the ''coast'' along the step and appears to become a stationary flow. In the left-handed geometry, four cases are presented. In cases (a), (b), and (c), it appears that a stationary ''offshore'' current is established, although somewhat broader and more irregular than in the right-

hand geometry case. Case (d) was somewhat peculiar since there was an acceleration applied to the coastal current. The response of the flow along the step was to break up into a train of eddies. Perhaps there is some indication here of an instability in the left-handed geometry and/or perhaps there is some connection with the variations along the topography that we saw in Fig. 15. It would be interesting to study further these results by performing simulations with shallow-water equations with the forcing and boundary conditions appropriate to the laboratory experiments, but that is beyond the scope of the present work.

We can now comment further on the oceanographic applications mentioned in the introduction. Qualitatively, our results suggest that we should see more small-scale variability when a coastal current crosses an escarpment at a coast in the case of left-handed geometries than in the case of right-handed geometries. The bifurcation of the Kuroshio north of Taiwan (Hsueh et al. 1992; Stern and Austin 1995) may be an example of this since it represents a case of a flow crossing a topographic step in a left-handed geometry, and, although it does tend to follow the shelf break in an offshore flow, there is a strong degree of variability. The ocean also provides some interesting examples of flow along a step in which the topographic contours run from one coast where the geometry of the step is right-handed to the opposite coast where the geometry is left-handed. In this situation, the flow leaving the ''right-handed boundary'' provides the source for the inshore flow to the ''left-handed boundary,'' and a circulation pattern is established in the direction predicted by the stationary quasigeostrophic theory. An example of such a current pattern may be seen in the vicinity of the Iceland–Faeroe Ridge. Hansen and Meincke (1979) show a bottom current pattern (see their Fig. 1) that does, to some extent, portray the bifurcations predicted by our quasigeostrophic stationary flow model. If we consider the northern side of the ridge as a step and the shelf breaks around Iceland and Faeroe island as coasts, then the flow pattern that Hansen and Meincke (1979; their Fig. 1) show agrees with the quasigeostrophic model predictions for the direction of the stationary barotropic current. The flow away from Iceland along the northern part of the ridge represents flow offshore in a right-handed geometry. The same flow then moves toward Faeroe Island where it represents inshore flow in a left-handed geometry. A similar analysis can be made for the flow along the southern slope of the ridge. In each case, the flow is in the direction of the predictions for steady flow according to the quasigeostrophic model. Another example is provided by the flow in the Adriatic Sea where the typical current pattern has a northward coastal current along the eastern boundary and a southward return flow along the western boundary. The Adriatic is shallow in the north and deep in the south with a strong transition occurring in the vicinity of the Jabuka Pit. This topographic feature bisects the Adriatic and is oriented perpendicularly to both eastern and western boundaries. Thus the geometry is right-handed on the eastern boundary and left-handed on the western boundary. The observed current across the middle of the Adriatic is again in the direction predicted by the quasigeostrophic steady-state flow. Finally, for the Bering slope current, we consider the schematic representation of current shown in Kinder et al. (1986, Fig. 5). We can suggest that the slope current, where it reaches the Russian coast, is the inshore flow predicted for steady left-handed geometries just as in Fig. 7c above, while that same current leaving the Aleutian chain, represents the offshore flow in the right-handed geometry as in Fig. 3c. (see also Kinder 1981; Kinder and Shumacher 1981). Our simple quasigeostrophic one-layer model cannot produce accurate quantitative approximations to the flow in these real oceanic flows. However, it may provide valuable guidance for further research with more complicated models on this question of coastal current bifurcations.

To summarize our results, there are some essential aspects of the coastal current interaction with an escarpment that we can emphasize. We have seen that the result of the interaction between the coastal current and the topography is determined by whether the geometry is right- or left-handed rather than by the direction of the coastal current. It makes little difference to the forms and strengths of the eddies generated by the interaction or to the direction of the flow along the slope whether the coastal flow experiences a step-up or a step-down when passing the escarpment, whereas the handedness of the geometry is critical. Also, in accord with a simple argument based on vortex tube stretching that we presented, in the left-handed geometry, the coastal current speed increases after passing the escarpment, while it decreases in the right-handed geometry, independent of coastal current direction. Further, the analytic stationary solution has an inshore flow along the escarpment for the left-handed geometry and an offshore flow for the right-handed geometry, again independent of the direction of the coastal current. Finally, we have shown that the reflection of the coastal current in the form of a dipolar jet back into the region upstream of the escarpment as observed by Stern and Austin (1995) occurs only in the left-handed geometry, whereas in the right-handed geometry the current either bifurcates with a portion flowing as a jet along the escarpment or, when the condition $|h_0/\omega_0| > 1$ is met, leaves the coast entirely and follows the escarpment.

Acknowledgments. This research has been supported in part by Office of Naval Research Grant N00014-96-1-0065. SGLS was funded by a Lindemann Trust Fellowship administered by the English Speaking Union. RP acknowledges support from CNR Short Term Fellowship and PRISMA2 grants. The numerical simulations were performed on IBM workstations at the University of Rome and the University of San Diego, and

on the C90 at the San Diego Super Computer Center. We thank Paolo Orlandi for providing the numerical simulation code and also for his very helpful advice. We thank Susan Allen for providing us with a copy of her thesis and a preprint of Allen and Hsieh (1997). We also thank GertJan van Heijst, Ted Johnson, Tom Kinder, Steve Ramp, and Melvin Stern for helpful suggestions.

APPENDIX

Inversion of the Fourier Transform

Here we present the details of the inversion of the contour integral used to obtain Eq. (22). We begin with

$$\tilde{g} = \frac{1}{l^2 + \lambda^2}[e^{-(l^2+\lambda^2)^{1/2}x} - 1]. \quad \text{(A1)}$$

The inverse transform is then

$$g(x, y) = \frac{1}{2\pi}\int_{-\infty}^{\infty} \frac{1}{l^2 + \lambda^2}[e^{-(l^2+\lambda^2)^{1/2}x} - 1]e^{ily}\, dl. \quad \text{(A2)}$$

We can perform this integral indirectly through the use of contour integration in the complex l plane (cf. Fig. A1). The integral that we need is the one on curve C_1. There are branch cuts from $\pm i\lambda$ to $\pm\infty$ and no singularities except for the branch points. The position of the branch cuts are picked to ensure that $(l^2 + \lambda^2)^{1/2}$ is positive and real along C_1. For positive y, Jordan's lemma can be invoked if we close the contour in the upper half-plane as shown in the figure. Since there are no singularities within the closed contour, the value of the integral on C_1 is the same as the negative of the combined values of the integrand on the other parts of the closed contour. Jordan's lemma implies that the contribution on C_2 and C_6 will vanish if we take the radii of those arcs to infinity. Also, the value of the integral on C_4 can be shown to vanish in the limit of the radius of that arc vanishing. This leaves the contributions from C_3 and C_5. Except for the factor $(l^2 + \lambda^2)^{1/2}$ the integrand is the same on both sides of the branch cut. To evaluate the $(l^2 + \lambda^2)^{1/2}$, we can first write $(l \pm i\lambda) = R_{\pm} \exp(i\theta_{\pm})$ using polar representations about the branch points at $l = \pm i\lambda$. Thus θ_- is $\pi/2$ on both C_3 and C_5, while θ_+ is $\pi/2$ on C_3 and $-3\pi/2$ on C_5. Thus we have $(l^2 + \lambda^2)^{1/2} = \pm i\sqrt{R_+R_-}$ with the plus sign for C_3. If we then define $l = iu$ on C_3 and C_5, we have $R_+ = u - \lambda$ and $R_- = u + \lambda$. Keeping track of signs, we can integrate along C_3 and C_5 to obtain

$$g = -\frac{1}{\pi}\int_{\lambda}^{\infty} \sin[x(u^2 - \lambda^2)^{1/2}]\frac{e^{-uy}}{u^2 - \lambda^2}\, du. \quad \text{(A3)}$$

Changing variables by $u = \lambda v$ leads to Eq. (22).

For negative y, in order to usefully apply Jordan's lemma, we must close the contour in the lower half-plane. By symmetry the answer must be the same with y replaced by $|y|$.

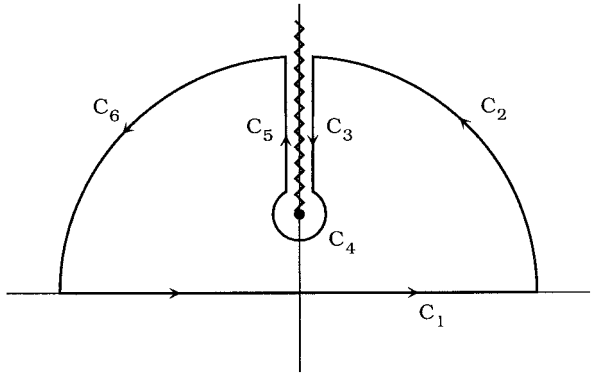

FIG. A1. Contour for performing the inverse Fourier transform needed to arrive at Eq. (22).

REFERENCES

Allen, S. E., 1988: Rossby adjustment over a slope. Ph.D. thesis, University of Cambridge, 205 pp.

——, 1996: Rossby adjustment over a slope in a homogeneous fluid. *J. Phys. Oceanogr.*, **26,** 1646–1654.

——, and W. W. Hsieh, 1997: How does the El Niño–generated coastal current propagate past the Mendocino escarpment? *J. Geophys. Res.* [*Oceans*], **102,** 24 977–24 985.

Bretherton, F. B., and D. B. Haidvogel, 1976: Two-dimensional turbulence above topography. *J. Fluid Mech.*, **78,** 129–154.

Carnevale, G. F., and J. S. Frederiksen, 1987: Nonlinear stability and statistical mechanics of flow over topography. *J. Fluid Mech.*, **175,** 157–181.

Carslaw, H. S., 1950: *An Introduction to the Theory of Fourier's Series and Integrals.* Dover, 368 pp.

Gel'fand, I. M., and G. E. Shilov, 1964: *Generalized Functions.* Academic Press, 423 pp.

Gill, A. E., M. K. Davey, E. R. Johnson, and P. F. Linden, 1986: Rossby adjustment over a step. *J. Mar. Res.*, **44,** 713–738.

Hansen, B., and J. Meincke, 1979: Eddies and meanders in the Iceland–Faroe Ridge area. *Deep-Sea Res., Part A (Oceanographic Research Papers),* **26,** 1067–1082.

Holloway, G., 1986: Eddies, waves, circulation, and mixing: Statistical geofluid mechanics. *Annu. Rev. Fluid Mech.,* **18,** 91–147.

Hsueh, Y., J. Wang, and C.-S. Chern, 1992: The intrusion of the Kuroshio across the continental shelf northeast of Taiwan. *J. Geophys. Res.*, **97,** 14 323–14 330.

Johnson, E. R., 1985: Topographic waves and the evolution of coastal currents. *J. Fluid Mech.,* **160,** 499–509.

——, and M. K. Davey, 1990: Free-surface adjustment and topographic waves in coastal currents. *J. Fluid Mech.,* **219,** 273–289.

Kinder, T. H., 1981: A perspective of physical oceanography in the Bering Sea, 1979. *The Eastern Bering Sea Shelf: Oceanography and Resources,* D. W. Hood and J. A. Calder, Eds., University of Washington Press, 5–13.

——, and J. D. Shumacher, 1981: Circulation over the continental shelf of the southeastern Bering Sea. *The Eastern Bering Sea Shelf: Oceanography and Resources,* D. W. Hood and J. A. Calder, Eds., University of Washington Press, 53–75.

——, D. C. Chapman, and J. A. Whitehead, 1986: Westward intensification of the mean circulation on the Bering Sea shelf. *J. Phys. Oceanogr.* **16,** 1217–29.

LeBlond, P. H., and L. A. Mysak, 1978: *Waves in the Ocean.* Elsevier, 602 pp.

Longuet-Higgins, M. S., 1968: Double Kelvin waves with continuous depth profiles. *J. Fluid Mech.,* **34,** 49–80.

Messiah, A., 1961: *Quantum Mechanics.* John Wiley and Sons, 1136 pp.

Orlanski, I., 1976: A simple boundary condition for unbounded hyperbolic flows. *J. Comput. Phys.,* **21,** 251–269.

Pedlosky, J., 1965: A note on the western intensification of the ocean circulation. *J. Mar. Res.,* **23,** 207–209.

——, 1996: *Ocean Circulation Theory.* Springer-Verlag.
Peyret, R., and T. D. Taylor, 1983: *Computational Methods for Fluid Flow.* Springer-Verlag, 358 pp.
Pond, S., and G. L. Pickard, 1978: *Introductory Dynamic Oceanography.* Pergamon, 329 pp.
Poulain, P.-M., 1997: Drifter observations of surface circulation in the Adriatic Sea between December 1994 and March 1996. *J. Mar. Syst.,* submitted.
Rai, M. M., and P. Moin, 1991: Direct simulations of turbulent flow using finite-difference schemes. *J. Comput. Phys.,* **96,** 15–53.
Rhines, P. B., 1969: Slow oscillations in an ocean of varying depth: Part 1. Abrupt topography. *J. Fluid Mech.,* **37,** 161–205.
Roache, P. J., 1972: *Computational Fluid Dynamics.* Hermosa, 434 pp.
Salmon, R., G. Holloway, and M. C. Hendershott, 1976: The equilibrium statistical mechanics of simple quasi-geostrophic models. *J. Fluid Mech.,* **75,** 691–703.
Spitz, Y. H., and D. Nof, 1991: Separation of boundary currents due to bottom topography. *Deep-Sea Res.,* **38,** 1–20.
Stern, M. E., and J. A. Whitehead, 1990: Separation of a boundary jet in a rotating fluid. *J. Fluid Mech.,* **217,** 41–69.
——, and J. Austin, 1995: Entrainment of shelf water by a bifurcating continental boundary current. *J. Phys. Oceanogr.,* **25,** 3118–3131.
Thompson, L., and G. R. Flierl, 1993: Barotropic flow over finite isolated topography: Steady solutions on the beta-plane and the initial value problem. *J. Fluid Mech.,* **250,** 553–586.
Willmott, A. J., and R. H. J. Grimshaw, 1991: The evolution of coastal currents over a wedge-shaped escarpment. *Geophys. Astrophys. Fluid Dyn.,* **57,** 19–48.